A Highly Sensitive Sub-THz Slot Disk Resonator for Permittivity Sensing Applications

Sajjad Sabbaghi, *Graduate Student Member, IEEE*, Hai Yu, Xuan Ding, *Member, IEEE*, Zahra Mohseni, *Graduate Student Member, IEEE*, and Qun Jane Gu, *Senior Member, IEEE*

***Abstract*—This letter presents the design and implementation of a highly sensitive slot disk resonator (SDR)-based sensor for permittivity sensing applications at sub-THz frequencies. The sensor utilizes a silicon waveguide (SiWG) on a quartz substrate. The slot within the disk enhances the horizontal electric field, thereby increasing the sensitivity of the sensor by promoting stronger interactions with the material under test (MUT). The measurement results demonstrate the sensitivity of 3.9 GHz/ε_r for 1-μL liquid MUTs.**

***Index Terms*—Coupling to dielectric waveguide (DWG), dielectric sensor, disk resonator, DWG, high-sensitive sensor, slot line to DWG, slot waveguide, sub-THz sensing.**

I. Introduction

DIELECTRIC sensing has a wide range of applications in agriculture, food industry, medical diagnosis, and environment monitoring [1]. It is also a powerful tool for monitoring and measuring the changes in the electrical properties of materials. Microwave sensing has been investigated for a long time using resonance, reflection, and transmission methods [2], [3], [4], [5], [6]. However, achieving a good sensing resolution for a tiny amount of material under tests (MUTs) is challenging at microwave frequencies. THz and sub-THz permittivity sensors, on the other hand, have been utilized in permittivity sensing applications, enabling the detection of minute quantities of various materials due to their compact dimensions [7], [8], [9]. The implementation of sub-THz sensor using silicon waveguide (SiWG) is one of the most efficient ways in terms of high resolution, small size, and low cost. The ring-resonator-based sensor is a well-known method for sensing in THz frequencies, where the electromagnetic field is confined within the ring at a specific frequency. The circulation of waves inside the ring enhances resonance, resulting in a higher quality factor ($Q = (f_{res}/\text{BW})$). However, the most challenging feature of a dielectric sensor is sensitivity, which can be present as the ability of the sensor to detect the changes of the input properties. It is one of the limitations of recent sub-THz sensors to achieve low resolution [8], [9]. The slot WG-based ring resonator is among the effective methods for enhancing sensitivity that have been used in optical domain [10], [11]. It features a narrow slot region between two SiWG ridges, where the horizontal electric field (E_x) is tightly confined. This configuration generates a strong evanescent field that extends beyond the WG core and improves sensitivity. However, slot WG mode excitation usually requires two transition steps, transition from E_y to E_x mode and from ridge WG to slot WG, which can introduce losses and increase the overall length of the sensing system.

This letter demonstrates a SiWG SDR-based sensor for permittivity sensing to improve the sensitivity of sub-THz sensors. The proposed SDR-based sensor improves the resolution of the sensor through enhanced interaction between the evanescent field and MUT. Also, a novel transition from a slot line to a SiWG is proposed, enabling the direct excitation of the E_x field within the WG. Additionally, a coupling mechanism between a ridge WG and the slot disk resonator (SDR) is introduced to excite slot mode inside the disk while minimizing the system losses and reducing the overall sensor dimensions.

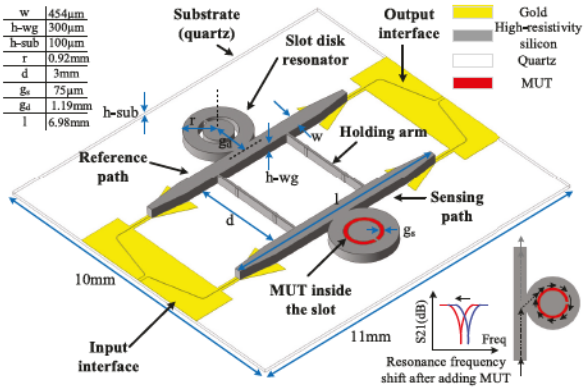

Fig. 1. Sensor structure.

II. Design of Sensing System

The proposed sensor system is shown in Fig. 1, which includes the sensor part and interfaces for the transition from transmission lines (TLs) to SiWGs. The sub-THz signal from the input interface is divided into the sensing and reference paths, both composed of SiWGs, before being recombined at the output interface. Quartz is used as the substrate due to its low loss and high-precision lithography, making it well-suited for THz frequencies. To enable the placement and guidance of liquid MUTs within the slot, a disk resonator with a slot is proposed as an alternative to the conventional slot ring resonator [10], [12]. This design simplifies the measurement process and minimizes the amount of required liquid MUT. The bidirectional system has two ports to excite and demultiplex E_{X11} mode and demultiplex E_{X11} mode in SiWGs. The system has a specific resonance frequency, and it will be

Received 20 April 2025; accepted 3 May 2025. This work was supported in part by COGNISENSE, one of the seven centers in JUMP 2.0, a Semiconductor Research Corporation (SRC) Program sponsored by DARPA, and in part by the National Science Foundation (NSF) under Grant 2314932. *(Corresponding author: Qun Jane Gu.)*

Sajjad Sabbaghi, Zahra Mohseni, and Qun Jane Gu are with the Department of Electrical and Computer Engineering, Georgia Institute of Technology, Atlanta, GA 30332 USA (e-mail: jane.gu@gatech.edu).

Hai Yu is with NVIDIA Corporation, Santa Clara, CA 95051 USA.

Xuan Ding is with the Department of Electrical and Computer Engineering, University of California Davis, Davis, CA 95616 USA.

Digital Object Identifier 10.1109/LMWT.2025.3567846

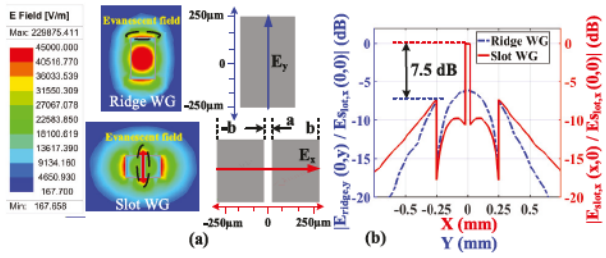

Fig. 2. (a) Comparison of the E-field magnitude for ridge and slot WGs (the pictures are front view of WGs) and (b) normalized E-field in terms of x- and y-axes for slot and ridge WGs, respectively.

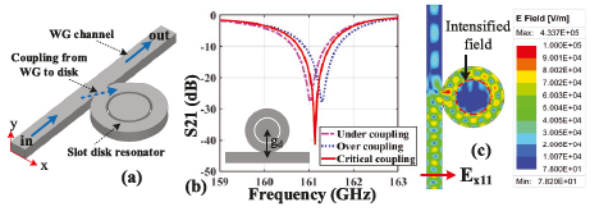

Fig. 3. (a) Sensor part of the system, (b) critical coupling simulation, and (c) simulated magnitude of E-field distribution from the top view in critical coupling.

changed after adding MUT on the sensing path because the resonance frequency is a function of effective permittivity of the resonator, MUT, and surrounding environment. To ensure accurate sensing irrespective of temperature and mechanical variations, the sensor employs two sensing and reference arms, each with its own resonance frequency. The reference path maintains a constant resonance frequency, while the sensing path's frequency varies based on the MUTs. After out-of-phase recombination at the output Y-junction, the overall system's resonance frequency falls between the two individual frequencies. The results from these arms are subtracted at the output interface to compensate for potential discrepancies.

A. Sensor

The sensor part is the main block of the system, which includes two similar sensing and reference paths. The sensing area of the system is located inside the slot of the disk. The relative permittivity (ε_r) is the main properties of MUT for the detection because it can make a frequency shift (f_r) in the resonance frequency of the disk resonator [8]

$$f_r = \frac{mc}{2\pi r\sqrt{\varepsilon_{r,\text{eff}}}} \tag{1}$$

where m is the number of wavelengths traveling inside the disk resonator, c is the speed of light, r is the radius of the disk, and $\varepsilon_{r,\text{eff}}$ is the effective permittivity of the sensor system and MUT. Larger electric field intensity in the sensing area results in more interaction of MUT and the sensor, thereby larger change in $\varepsilon_{r,\text{eff}}$ of the system and higher frequency shift (1). Therefore, larger E-field in the sensing area can improve the sensitivity of the system, which can be written as

$$S_{\text{sens}} = \frac{\partial f_r}{\partial \varepsilon_r}. \tag{2}$$

To explain the effect of the SDR in comparison with the simple ring resonator, a comparison between the evanescent field of slot WG and ridge WG is presented. Fig. 2(a) shows the electric field magnitude between two WGs. For the ridge WG, most of the electric field is concentrated within the channel, with the evanescent field, primarily extending above and below the WG where the MUT would be placed. In contrast, for the slot WG, most of the electric field is confined within the slot itself, where the liquid MUT can penetrate. The E_x-component

$$E_x(x) = A\begin{cases} \dfrac{1}{\varepsilon_{\text{slot}}}\cosh(\gamma_{\text{slot}}x); & |x| < \dfrac{a}{2} \\ \dfrac{1}{\varepsilon_{\text{si}}}\cosh(\gamma_{\text{slot}}a)\cos(\gamma_{\text{si}}(|x|-a)) + \dfrac{1}{\varepsilon_{\text{slot}}}\dfrac{\gamma_{\text{slot}}}{\gamma_{\text{si}}} & \\ \quad \times \sinh(\gamma_{\text{slot}}a)\sin(\gamma_{\text{si}}(|x|-a)) & \\ & \dfrac{a}{2} < |x| < \dfrac{b}{2} \end{cases} \tag{3}$$

of the slot WG can be written as (3) [11], where γ_{slot} and γ_{si} are the propagation constants of wave inside the slot and WG. Also, a and b are the width of slot and the whole WG. It can be shown that if $x = a$ at the boundary of slot and WG, the evanescent field is significantly enhanced by a factor of $\varepsilon_{\text{si}}/\varepsilon_{\text{slot}}$, where ε_{si} and $\varepsilon_{\text{slot}}$ represent the permittivity of silicon and air in this case. Considering the permittivity of high-resistivity silicon, the E-field can be intensified by 11.7 times. The normalized electric field for the ridge and slot WGs along the y- and x-axes, respectively, is shown in Fig. 2(b). The normalized electric field of slot waveguide within the slot ($|x| < a$) is almost 7.5 dB higher than the one at the edges of ridge WG (250 μm bottom and top). This intensified evanescent field shows the potential of the slot WG for sensitivity improvement. The main part of the system, sensor, is shown in Fig. 3(a). The slot waveguide mode is excited by a ridge WG that has E_x mode instead of conventional transition from another slot WG, thereby decreasing the system's loss. The distance between the center of the disk to the center of the channel (g_d) is optimized to make the critical coupling happen [Fig. 3(b)]. That is where the total energy transferred to the resonator precisely matches the intrinsic losses within the resonator, and the transmission drops to zero. The frequency that the critical coupling happens is around 161.1 GHz, as shown in the figure. The simulated magnitude of the E-field distribution at the resonance frequency is illustrated in Fig. 3(c). As shown, the intensity of field inside the slot is higher than high index material, silicon. As a result, the sensitivity can be improved by the interaction of MUT with the intensified E-field inside the slot.

B. Input and Output Interface

Fig. 4(a) illustrates the system's interface, transitioning from a 50-Ω coplanar waveguide (CPW) to SiWG. The input port feeds a Y-junction slot line power divider for both sensing and reference paths. The power divider's output arms are out-of-phase with 100-Ω impedance for matching. A slot line is used for in-line excitation of the SiWG, as it supports an odd mode with a dominant symmetric horizontal E-field. This field aligns with the required field in the SiWG, maximizing mode coupling efficiency ($\propto \vec{E}_{\text{slot}}.\vec{E}_{\text{SiWG}}$) [Fig. 4(a) and (b)]. A new slot line to SiWG transition is proposed to enhance the system interface, utilizing tapered ends for impedance matching. Fig. 4(c) demonstrates the low-loss characteristics of the power divider and slot line to SiWG coupling. Fig. 4(d)

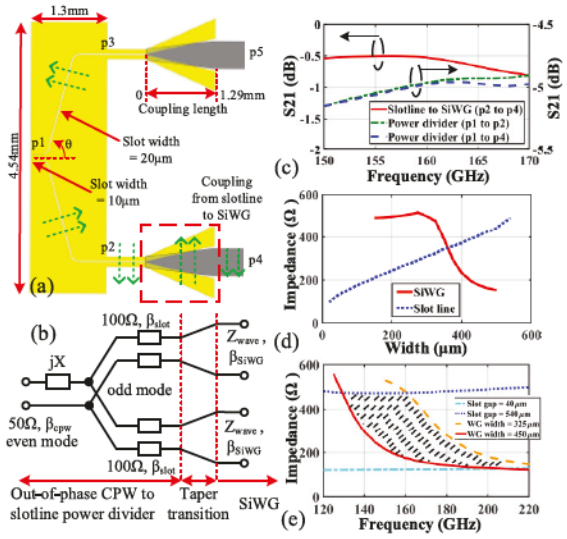

Fig. 4. (a) Top view of system's interface, (b) circuit model of transitions, (c) loss of power divider and slot line to SiWG coupling, (d) characteristic impedance of slot line and SiWG versus their width variations, and (e) characteristic impedance versus frequency for different widths of slot line and SiWG.

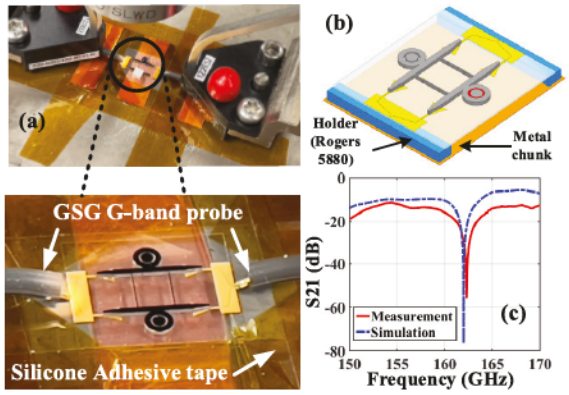

Fig. 5. (a) Sensor attached to the chunk in the measurement setup and connected to a pair of GSG G-band probe, (b) picture of the system with holders, and (c) S_{21} of the system before adding MUT.

shows how the characteristic impedance of both SiWG and slot line varies with width changes—slot line impedance increases with slot width, while SiWG impedance rises as its width decreases. Additionally, varying the slot gap (40–540 μm) and the SiWG width (325–450 μm) over the coupling length ensures wideband matching (130–210 GHz), as highlighted in the shaded area of Fig. 4(e).

III. Fabrication and Measurement Results

A 300-μm-thick high-resistivity silicon wafer is etched to form the dielectric sensor. Input and output interfaces are fabricated separately and attached to the sensor using paste and die-bond equipment (FinTech Fine Placer). The complete system is shown in Fig. 5(a) and (b), with low-loss Rogers 5880 material used as holders for measurements. Fig. 5(c) indicates a resonance frequency of approximately 162.3 GHz before adding sample on the sensing path, and the measured Q is 4050. Two different types of MUTs, solid and liquid, are chosen to be measured by the sensor. All materials have close relative permittivity to show the highly sensitive capability

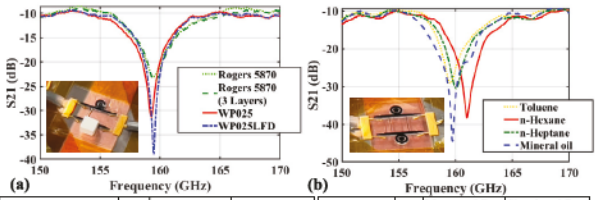

Solid MUT	ε_r	Measured Res. Freq. (GHz)	Simulated Res. Freq. (GHz)
Rogers 5870 (1 layer)	2.33	159.48	159.75
Rogers 5870 (3 layers)	2.33	159.56	159.85
WP025 LFD	2.5	159.41	159.68
WP025	2.55	159.27	159.57

Liquid MUT	ε_r	Measured Res. Freq. (GHz)	Simulated Res. Freq. (GHz)
n-Hexane	1.88	161	160.9
n-Heptane	1.92	160.2	160.67
Mineral oil	2.2	159.75	159.81
Toluene	2.38	159.5	159.67

Fig. 6. Measured S_{21} for (a) solid MUTs and (b) liquid MUTs.

TABLE I
Papers Comparison With Recent State-of-the-Art Resonance-Based Permittivity Sensors at Different Spectra

Reference	[2], 2020	[3], 2024	[4], 2025	[5], 2020	[8], 2018	[13], 2021	This work
Method	CSRR	CSRR	CCSRR	CSSR	Dielectric ring	Double slot MRR	Dielectric slot disk
Frequency	2.24 GHz	2.46 GHz	2.26 GHz	14 GHz	165 GHz	193.4 THz	162 GHz
Sensor size (mm^2)	76.16	1320	500	36	1	0.0001	3.61
MUT size (mm^3)	79.2	2.32	400	100	0.38	NA	1
Quality factor[1]	1119	18.5	252	501	84	4325	4050
Sensitivity (MHz/ε_r)	80	1.37	82	1028	600	433 nm/RIU	3900
MUT type	Solid & liquid	Liquid	Solid	Solid	Solid & liquid	Liquid	Liquid preferably
Planar integration	Easy	Easy	Easy	Easy	Easy	Hard	Easy

[1]*Unloaded Q based on measurement results*

of the sensor for small amounts of MUTs. As shown in Fig. 6(a), resonance frequency shifts are smaller for solid samples than for liquid samples [Fig. 6(b)] due to the horizontal electric field being concentrated in the gap, where liquids can penetrate, rather than on top of the disk, where solid MUTs are placed. A pipette is used to dispense 1 μL of liquid onto the sensor. Also, isopropyl alcohol (IPA) is used to clean the sensor after each measurement. The sensor's sensitivity for liquid MUTs, comparing n-hexane and mineral oil, is approximately 3.9 GHz/ε_r. A comparison with other state-of-the-art permittivity sensors is summarized in Table I. Based on the comparison results in the table, the proposed sensor exhibits higher sensitivity than microwave and sub-THz sensors while maintaining a high-quality factor. This improved quality factor enhances the system's resolution, as resolution is inversely proportional to the sensor's Q-factor and sensitivity [8].

IV. Conclusion

This letter proposes a high-sensitivity SDR-based sensing system, implemented to enhance precision and performance. By employing a slot within the disk resonator, the system achieves intensified interaction with the MUT, significantly boosting sensitivity. The horizontal electric field in the WG effectively excites the slot WG mode. Additionally, the bidirectional design, featuring dual reference and sensing paths, ensures robust and accurate sensing capabilities.

References

[1] K. Entesari, A. A. Helmy, and M. Moslehi-Bajestan, "Integrated systems for biomedical applications: Silicon-based RFmicrowave dielectric spectroscopy and sensing," *IEEE Microw. Mag.*, vol. 18, no. 5, pp. 57–72, Jul. 2017.

[2] H. Gan et al., "A CSRR-loaded planar sensor for simultaneously measuring permittivity and permeability," *IEEE Microw. Wireless Compon. Lett.*, vol. 30, no. 2, pp. 219–221, Feb. 2020.

[3] X. Han et al., "Highly integrated improved hexagonal CSRR-based fluid sensor for complex dielectric parameter detection," *IEEE Sensors J.*, vol. 24, no. 13, pp. 20559–20570, Jul. 2024.

[4] A. Hanif et al., "Compact complementary highly sensitive microwave planer sensor for reliable material dielectric characterization," *IEEE Sensors J.*, vol. 25, no. 3, pp. 4749–4756, Feb. 2025.

[5] T. Haq, C. Ruan, X. Zhang, S. Ullah, A. K. Fahad, and W. He, "Extremely sensitive microwave sensor for evaluation of dielectric characteristics of low-permittivity materials," *Sensors*, vol. 20, no. 7, p. 1916, Mar. 2020.

[6] C. Ding et al., "Multiband permittivity measurement using directional coupler based on groove–ridge-gap waveguide," *IEEE Trans. Instrum. Meas.*, vol. 73, pp. 1–10, 2024.

[7] A. Sarkaleh, B. Lahijani, H. Saberkari, and A. Esmaeeli, "Optical ring resonators: A platform for biological sensing applications," *J. Med. Signals Sensors*, vol. 7, no. 3, p. 185, 2017.

[8] B. Yu, X. Ding, H. Yu, Y. Ye, X. Liu, and Q. J. Gu, "Ring-resonator-based sub-THz dielectric sensor," *IEEE Microw. Wireless Compon. Lett.*, vol. 28, no. 11, pp. 969–971, Nov. 2018.

[9] H. Yu, X. Ding, J. Chen, S. Sabbaghi, and Q. J. Gu, "Design and analysis of a sub-THz resonator-based high-resolution permittivity sensor," *IEEE Trans. Microw. Theory Techn.*, vol. 72, no. 5, pp. 2809–2823, May 2024.

[10] E. Luan, H. Shoman, D. M. Ratner, K. C. Cheung, and L. Chrostowski, "Silicon photonic biosensors using label-free detection," *Sensors*, vol. 18, no. 10, p. 3519, Oct. 2018.

[11] V. R. Almeida, Q. Xu, C. A. Barrios, and M. Lipson, "Guiding and confining light in void nanostructure," *Opt. Lett.*, vol. 29, no. 11, p. 1209, Jun. 2004.

[12] N. L. Kazanskiy, S. N. Khonina, and M. A. Butt, "Subwavelength grating double slot waveguide racetrack ring resonator for refractive index sensing application," *Sensors*, vol. 20, no. 12, p. 3416, Jun. 2020.

[13] C. Liu, C. Sang, X. Wu, J. Cai, and J. Wang, "Grating double-slot microring resonator for sensing," *Opt. Commun.*, vol. 499, Nov. 2021, Art. no. 127280.